

Notes on Ocean Eddy Diffusivity

C. B. Rocha* & W. R. Young

March 7, 2016

1 The Advection-Diffusion Equation

1.1 Preliminaries

We are concerned with the lateral advection and diffusion of a passive scalar (tracer). The evolution of the tracer concentration θ is governed by

$$\theta_t + \vec{u} \cdot \nabla \theta = \mathcal{S} + \kappa \Delta \theta, \quad (1)$$

where \mathcal{S} represents sources, κ is the molecular diffusivity of the tracer θ , and the horizontal laplacian is $\Delta \stackrel{\text{def}}{=} \partial_x^2 + \partial_y^2$. The advection-diffusion equation above is also often written as and (1) can be re-written

$$\theta_t + J(\psi, \theta)\theta = \mathcal{S} + \kappa \Delta \theta, \quad (2)$$

where the horizontal Jacobian is $J(A, B) = A_x B_y - B_x A_y$, and the streamfunction ψ , associated with the non-divergent flow \vec{u} , is defined by

$$u = -\psi_y, \quad \text{and} \quad v = \psi_x. \quad (3)$$

1.2 Zonally-averaged Equations

For application in simple periodic domain, it is convenient to introduce zonally-averaged equations. In more complicated geometries, similar decompositions can be achieved given a well-defined average, which in practice is a combination of time and space averaging. Introducing the Reynolds decomposition

$$\theta(x, y, t) = \langle \theta \rangle_x(y, t) + \theta'(x, y, t), \quad (4)$$

$$\psi(x, y, t) = \langle \psi \rangle_x(y, t) + \psi'(x, y, t), \quad (5)$$

where

$$\langle f \rangle_x(y, t) = \frac{1}{L_x} \int_0^{L_x} f(x, y, t) dx. \quad (6)$$

With periodicity in x , the x -averaged y -velocity vanishes $\bar{v} = \bar{\psi}_x = 0$. The x -averaged tracer equation is then

$$\partial_t \langle \theta \rangle_x + \partial_y \langle v' \theta' \rangle_x = \langle S \rangle_x + \kappa \partial_y^2 \langle \theta \rangle_x. \quad (7)$$

For completeness, the equation for the perturbation about the x -averaged tracer is

$$\theta'_t + \partial_x(u'\theta') + \partial_y(v'\theta') + \partial_x(u'\langle \theta \rangle_x) + \partial_y(v'\langle \theta \rangle_x) - \partial_y \langle v' \theta' \rangle_x = S' + \kappa(\partial_y^2 \theta' + \partial_x^2 \theta). \quad (8)$$

*Scripps Institution of Oceanography, University of California, San Diego. E-mail: crocha@ucsd.edu

1.3 Eddy diffusion

This notes discusses different methods for estimating ocean eddy diffusivities. A common heuristic argument is parameterize eddy transport such as $\bar{v}'\bar{\theta}'$ with a down-gradient eddy-difussivity

$$\bar{v}'\bar{\theta}' = -\kappa_e \partial_y \bar{\theta}. \quad (9)$$

The introduction of the eddy diffusivity (9) needs to be justified more formally. For now, it suffices to mention that (9) is a good approximation provided there is enough scale separation between the large-scale tracer gradient the eddy scales. Thus the parameterization (9) is used to close the zonally-averaged equation (7):

$$\bar{\theta}_t = \bar{S} + \kappa_{tot} \partial_y^2 \bar{\theta}, \quad (10)$$

where the total diffusivity is $\kappa_{tot} \stackrel{\text{def}}{=} \kappa_e + \kappa$. There is significant inconsistency in the literature regarding notation and naming of diffusivities. The term “effective diffusivity” is used to refer to κ_{tot} by some authors. Other investigators refer to κ_e as the “effective diffusivity” likely recognizing that for large Peclet number $\kappa_{tot} \approx \kappa_e$. The term “eddy diffusivity” is equally used to refer to both κ_{tot} or κ_e .

1.4 Integral variance budget

With harmless boundary conditions (e.g., double periodicity or no-flux across the boundaries) the tracer variance equation is

$$\frac{d}{dt} \int \frac{1}{2} \theta^2 dA = \int \theta S dA - \kappa \int |\nabla \theta|^2 dA. \quad (11)$$

2 Renovated Waves on a Lattice

To begin exploring the accuracy of different methods to estimate ocean eddy diffusivities, we use a simple advection-diffusion model on a lattice first proposed by Pierrehumbert (2000). The idea is to break the advection and difussion in different steps. The advection step is further separated in two sub-steps: advection in the x-direction and y-direction. The advection sub-steps are performed on a lattice. That is, the advection in the x-direction corresponds to a shift in the x-direction, and the advection in the y-direction corresponds to a shift in the y-direction:

$$i_x^{n+1} = i_x^n - \text{int}[u(y)\tau/2], \quad (12)$$

and

$$i_y^{n+1} = i_y^n - \text{int}[v(x)\tau/2], \quad (13)$$

where the superscripts represent the iteration and τ is the length of the renovation cycle, typically a eddy-turnover timescale. Figure 1 illustrates the advection sub-steps in a couple of renovation cycles. Clearly, a very complex tracer pattern emerges after a couple of renovation cycles. Notice that this advection scheme exactly conserves the probability density of the tracer if no diffusion is applied (the lattice is just re-combined).

In a slight generalization of Pierrehumbert’s model, we represent the non-divergent velocity field as linear combination of a spectrum of waves with random phase:

$$u(y) = C \sum_{j=j_{min}}^{j_{max}} \left(\frac{j}{j_{min}} \right)^{-p/2} \cos \left(\frac{2\pi y}{L_y} j + \phi_j \right), \quad (14)$$

$$v(x) = C \sum_{j=j_{min}}^{j_{max}} \left(\frac{j}{j_{min}} \right)^{-p/2} \cos \left(\frac{2\pi x}{L_x} j + \psi_j \right), \quad (15)$$

where L_x and L_y are the dimensions of the periodic domain, ψ_n and ϕ_n are random phases drawn from a uniform distribution on $[0, 2\pi]$. Because these random phases are changed every iteration, this simple velocity field is termed renovated wave model. Note that in this generalized renovated wave model the kinetic energy spectrum of the flow follows a j^{-p} power-law. Also in (14) and (15), C is a normalization constant, determined so that the root-mean square velocity is prescribed

$$C = 2u_{rms} \left(\sum_{j=j_{min}}^{j_{max}} \left(\frac{j}{j_{min}} \right)^{-p} \right)^{-1/2}. \quad (16)$$

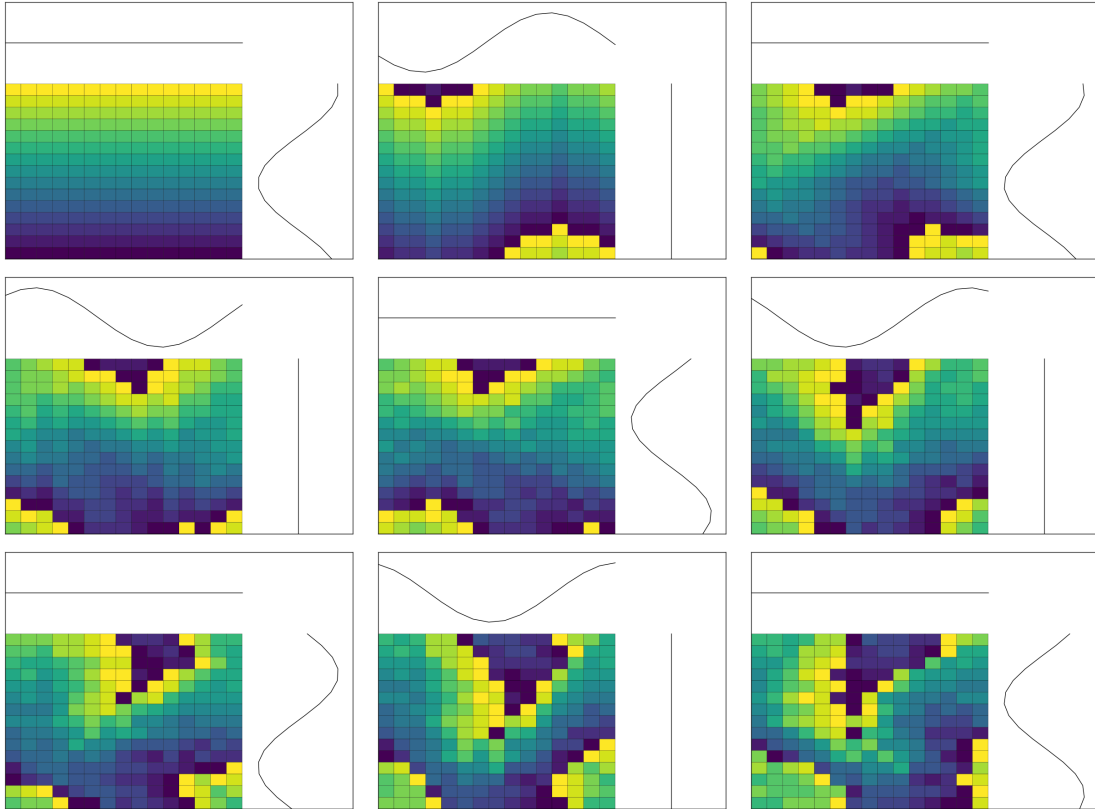


Figure 1: The advection on the two-dimensional periodic lattice. Notice that a complex pattern starts to emerge after a couple of renovation cycles. With a bigger lattice, one no longer sees the pixel fragmentation, and the differential advection results in strong filamentation.

Pierrehumbert performs the diffusion step in physical space, as a simple average of neighboring points, corresponding to a second-order finite-difference approximation for the laplacian operator. Here we take advantage of the periodicity of this model, and perform the diffusion step more accurately in Fourier space:

$$\hat{\theta}_{k,l}^{n+1/2} = \hat{\theta}_{k,l}^n e^{-\kappa(k^2+l^2)\tau/2}. \quad (17)$$

2.1 Advection-diffusion with constant background tracer gradient

Instead of using a large-scale source, we implement a constant background gradient G , so that the tracer concentration equation is

$$\theta_t + \vec{u} \cdot \nabla \theta + Gv = \kappa \Delta \theta. \quad (18)$$

The x -averaged variance budget is

$$\partial_t \langle \frac{1}{2} \theta \rangle_{x,t} + \partial_y \langle \frac{1}{2} v \theta^2 \rangle_{x,t} + G \langle v \theta \rangle_{x,t} = \partial_y^2 \langle \frac{1}{2} \theta^2 \rangle_{x,t} - \kappa \langle |\nabla \theta|^2 \rangle_{x,t}. \quad (19)$$

Because the background gradient is constant, the system is statistically homogeneous in y . Thus, in statistical steady state, the x -averaged variance budget (19) is exactly given by a balance between variance production and dissipation:

$$G\langle v\theta \rangle_{x,t} = -\kappa\langle |\nabla\theta|^2 \rangle_{x,t}. \quad (20)$$

2.2 Spectral characteristics of RW simulations

Our main interest is to use the lattice model to understand the potential biases and limitations of different methods to estimate eddy diffusivities, with particular attention to the dependence on the kinetic energy spectral slope. While the RW is simple enough to allow us to calculate its diffusivity exactly, its simulations display many characteristic of stirring and mixing by turbulent flows. In particular, the tracer dynamics dependence on the characteristics of the flow is well-represented in the RW model. Figure 2 shows spectra from two 8192×8192 RW simulations. With steep kinetic energy spectrum k^{-4} (c), the tracer stirring is spectrally non-local (dominated by the energy containing eddies $k_{min} = 1$). The tracer variance spectrum is very shallow, approximately following a k^{-1} power law across all scales. In contrast, with shallow kinetic energy spectrum k^{-2} (a), the tracer stirring is spectrally local, and the tracer variance spectrum approximately follow the same power law as the kinetic energy spectrum k^{-2} . At about the maximum wavenumber of the flow (the smallest stirring scale; $k_{max} = 150$), the tracer variance spectrum transitions to k^{-1} , Batchelor spectrum (see Vallis 2006; Scott 2006).

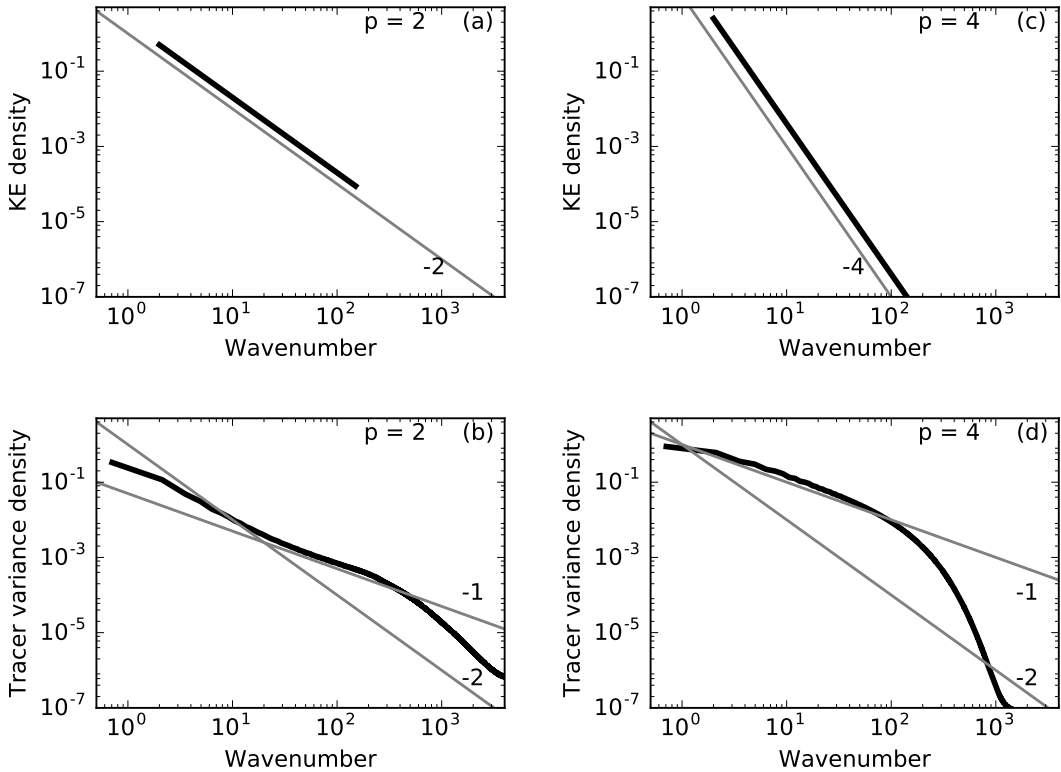


Figure 2: Kinetic energy spectra (a and c) and tracer variance spectra (b and d) from RW simulations with different spectral slopes of the kinetic energy. The simulations were run with same level of energy ($u_{rms}^2/2$) on a 8192×8192 lattice. In this experiments, the minimum stirring wavenumber is $k_{min} = 1$ and the maximum stirring wavenumber is $k_{max} = 150$.

2.3 The Osborn-Cox method

Cox and Osborn introduced an eddy diffusion closure for the tracer flux,

$$\langle v\theta \rangle_{x,t} = -\kappa_{oc}G, \quad (21)$$

to obtain an explicit expression for the eddy diffusivity

$$\kappa_{oc}(y) = \frac{\langle |\nabla\theta|^2 \rangle_{x,t}}{G^2} \kappa. \quad (22)$$

Note that the Osborn-Cox eddy diffusivity is simply an amplification of the molecular diffusivity, with the amplification factor

$$A_{oc} = \frac{\langle |\nabla\theta|^2 \rangle_{x,t}}{G^2}. \quad (23)$$

The amplification factor can be thought as a ratio of two length scales. In particular the perturbation of tracer scale as $\theta \sim l_{mix}G$, where l_{mix} is a mixing-length scale. Gradients of θ occur on relatively small scales extending down to the Batchelor scale,

$$l_b = \left(\frac{\kappa}{S}\right)^{1/2}, \quad (24)$$

where S is a characteristic scale of the rate of strain of the eddy field. Hence,

$$A_{oc} \sim \frac{l_{mix}^2}{l_b^2} \implies \kappa_{oc} \sim l_{mix}^2 S. \quad (25)$$

It is pleasing that the eddy diffusivity scaling (25) is independent of the molecular diffusivity κ .

2.4 The Nakamura method

A different approach to estimating the eddy diffusivity is the method of Nakamura). In particular, Nakamura showed that averaging the advection-diffusion equation (1) along tracer contours eliminates the advective eddy transport. The transformed equation resemble a diffusion equation in area coordinate with diffusivity (see appendix A for a derivation of the method):

$$K_n(\Theta, t) = L_{eq}^2 \kappa, \quad (26)$$

where L_{eq} is the equivalent length of the contour. K_N is an instantaneous measure of mixing as a function of each contour Θ ; K_{nit} has units of $(\text{length})^4 (\text{time})^{-1}$. The Nakamura eddy diffusivity is then defined as

$$\kappa_n(\Theta) = \langle K_n \rangle_t / L_{min}^2, \quad (27)$$

where L_{min} is the minimum length of the contour (L_x in this case). One generally maps the Nakamura diffusivity from contour Θ to physical space $\Theta = \Theta(y)$ either using the structure of the background tracer concentration (Gy) or by constructing a simple one-to-one map based on the distribution of the stirred tracer field.

2.5 RW model simulations

We now diagnose eddy diffusivities using both Osborn-Cox and Nakamura methods in reference simulations of the Renovated Waves (RW) model. The RW model implemented with background constant tracer concentration G is a plain-vanilla example of “Statistically Homogeneous Isotropic Transport” setup where the eddy diffusivity is given by Einstein’s formula

$$\kappa_{ein} = \frac{\langle (\Delta x)^2 \rangle}{2\tau}. \quad (28)$$

Table 1: Parameter of the RW experiments on a lattice.

Size of the lattice	$n_x = N_y = 4096$
Domain size	$L_x = L_y = 2\pi$
Velocity root-mean-square	$u_{rms} = 1$
Small scale diffusivity	$\kappa = 10^{-4}$
Eddy decorrelation time scale	$\tau = 0.5$
Peclet number	$Pe = 5 \times 10^3$

In the RW model we have

$$\dot{x} = u(y), \quad (29)$$

with $u(y)$ given by the series (14). Hence

$$\langle (\Delta x)^2 \rangle = \langle (x - x_0)^2 \rangle = u_{rms}^2 \tau^2 \langle \cos(l y + \psi_j) \rangle_\psi = \frac{u_{rms}^2 \tau^2}{2}. \quad (30)$$

Thus

$$\kappa_{ein} = \frac{u_{rms}^2 \tau}{4}. \quad (31)$$

Of course, in this case, the isotropic velocity field implies $\langle (\Delta x)^2 \rangle = \langle (\Delta y)^2 \rangle$ and the diffusivity is independent of direction.

Another important property of this model with constant background tracer gradient is that the scale separation between the mean tracer concentration and perturbations is infinite, and therefore the eddy diffusion closure is well justified.

2.6 Some results

Here we present results from two simulations akin of those figure 2 but with a little coarser resolution (4096×4096). Details in table 2.6.

Figure (3) shows variance time series for two experiments with the parameters described above but with distinct kinetic energy spectrum: $p = 2$ and $p = 4$. Both experiments achieve statistical steady state no later than about 20 renovation cycles — the diagnostics discussed below are calculated after equilibration. Figure 5 shows a snapshot of tracer concentration together with the probability density function of the tracer concentration. Also shown in figure 5 are the kinetic energy spectrum and the tracer spectrum ? the latter exhibits an approximate k^{-1} power law characteristics of non-local mixing. Results for the $p = 2$ experiments display different properties: the stirring is local in the range of active stirring and becomes non-local at wavenumbers larger than k_{max} (see the transition in the tracer spectrum in figure 6). The tracer concentration displays much rougher contours and its probability density function is less Gaussian than the one for the $p = 4$ experiment.

Figure (7) shows the x -averaged tracer variance budget and the estimates of eddy diffusivity. The tracer budget is nearly closed (inaccuracies are associated with the diffusion pulsing) and it is dominated by the balance between nearly y -independent production and dissipation, which are positive and negative definite, respectively. The other terms are smaller and integrate to zero. The estimates of eddy diffusivity are also essentially independent of y . The y -averaged value of both diffusivities calculated using Osborn-Cox and Nakamura method is about 1% accurate (more averaging and substeps within the renovation cycles could further reduce this inaccuracy). Figure 8 shows the tracer budget and eddy diffusivity for the $p = 2$ experiment. While in the $p = 2$ experiment the equilibrated tracer variance is about five times smaller than the variance in $p = 4$ experiment, the the production and dissipation rates are are the same (hence the same eddy diffusivity).

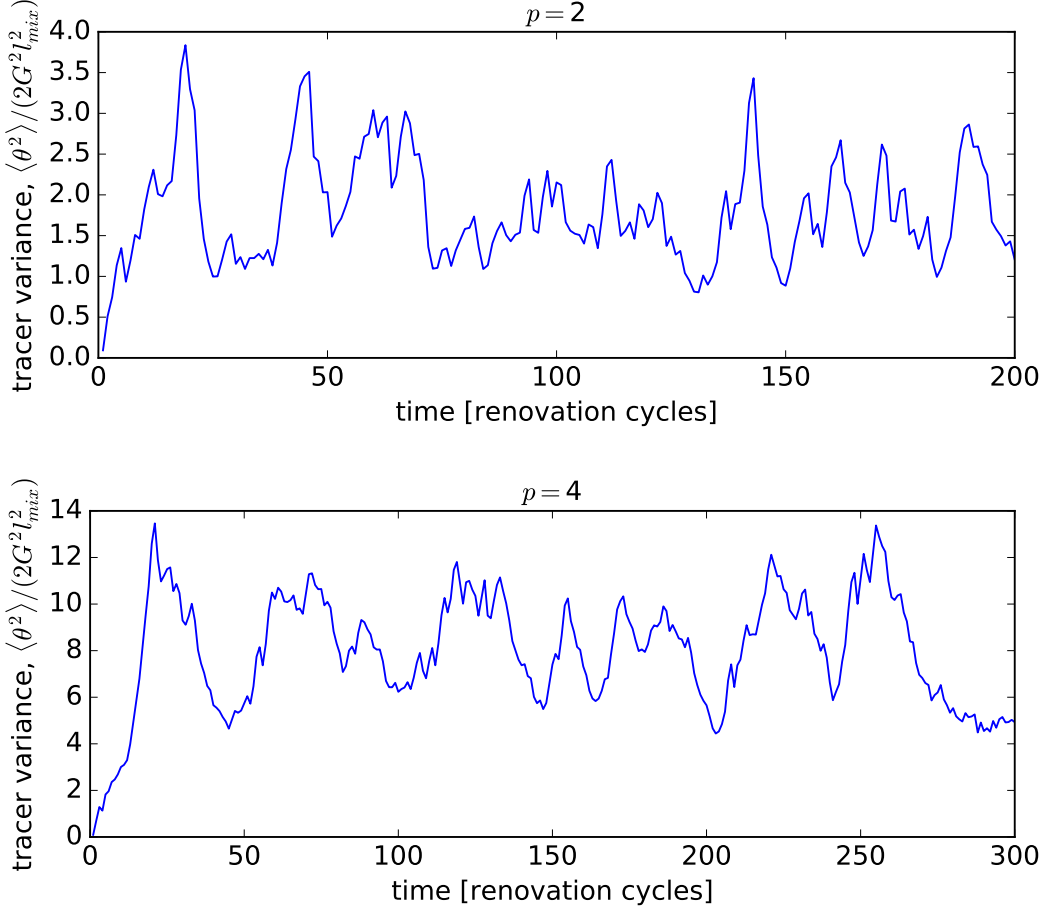


Figure 3: Results for RW simulations with $p = 2$ and $p = 4$. Notice the difference between the variance level in the two experiments.

While the eddy transport is the same, the tracer variance is much large in the $p = 4$ simulation. We can write the eddy tracer as

$$\langle v' \theta' \rangle_{xt} = \alpha(p) v_{rms} \theta'_{rms}(p), \quad (32)$$

where $\alpha(p)$ is a correlation coefficient. Since v_{rms} is prescribed as the same in both simulations, both the correlation coefficient α and the tracer rms θ'_{rms} are functions of the spectral exponent p . In particular, the results suggest that α be increasing larger for smaller p .

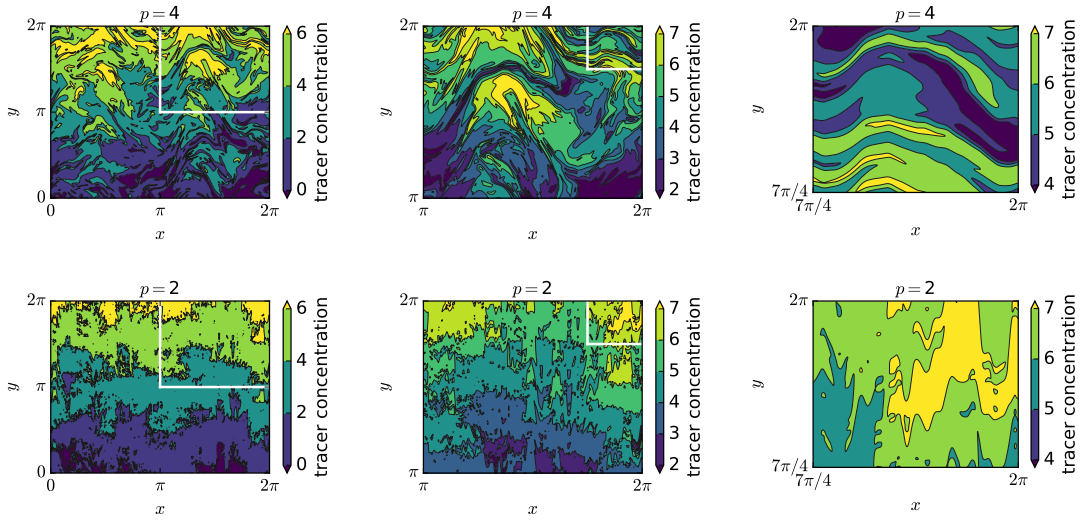


Figure 4: Snapshots for RW simulations with $p = 2$ (top) and $p = 4$ (bottom). Full domain (left), a quarter of the domain (middle), and one sixteenth of the domain (right).

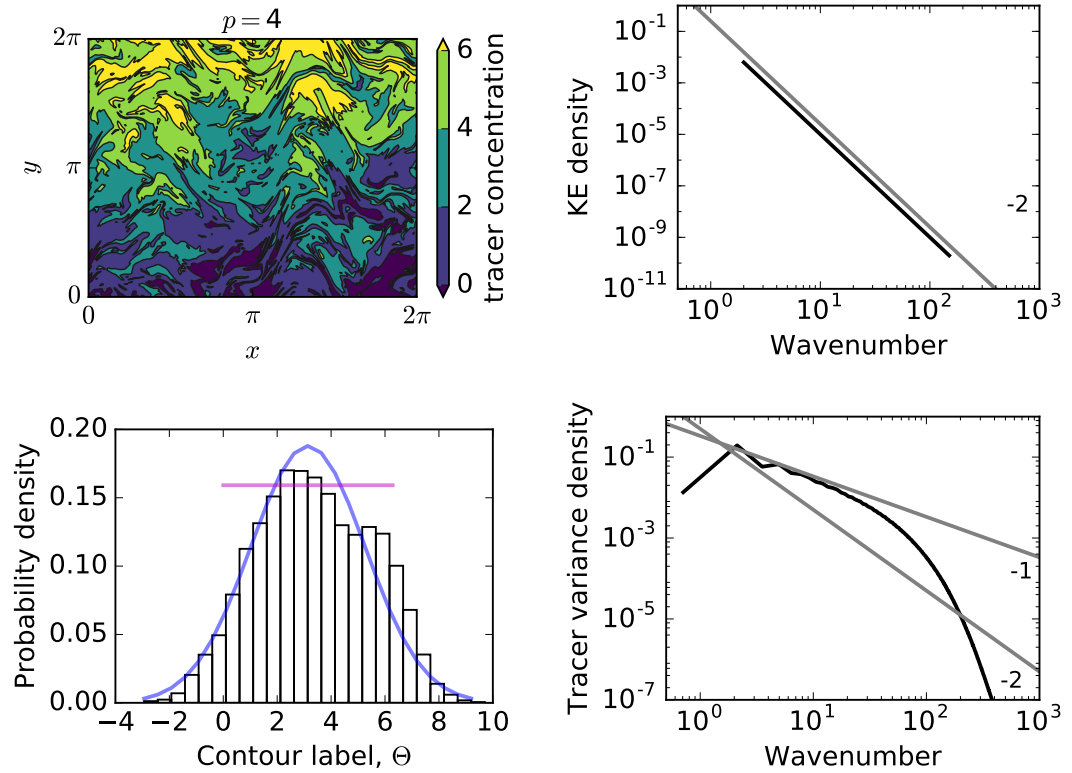


Figure 5: Results for $p = 4$ experiment. Snapshot of tracer concentration (top left) and associated probability density function (lower left). Kinetic energy spectrum (top right) and tracer variance spectrum (lower right).

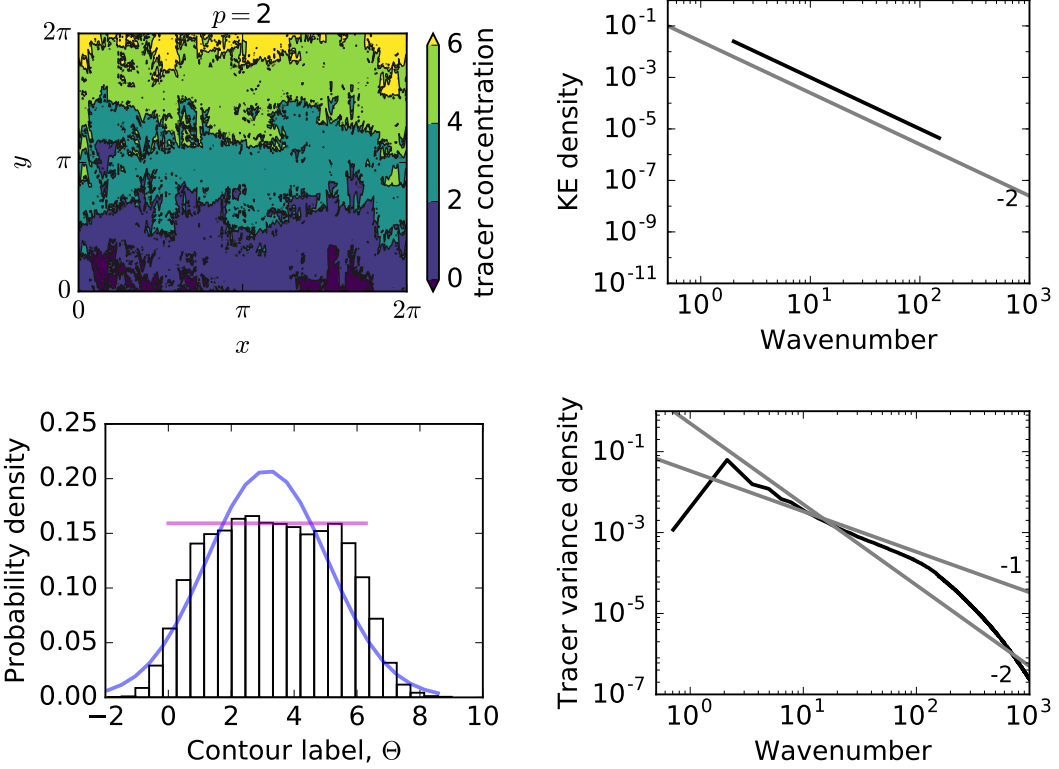


Figure 6: Results for $p = 2$ experiment: Snapshot of tracer concentration (top left) and associated probability density function (lower left). Kinetic energy spectrum (top right) and tracer variance spectrum (lower right).

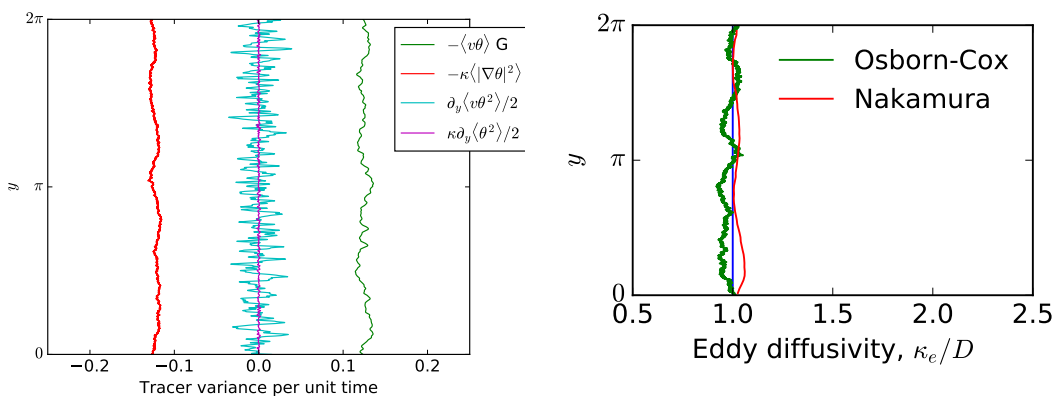


Figure 7: Results for $p = 4$ experiment: Tracer variance budget (left) and estimates of eddy diffusivity (right).

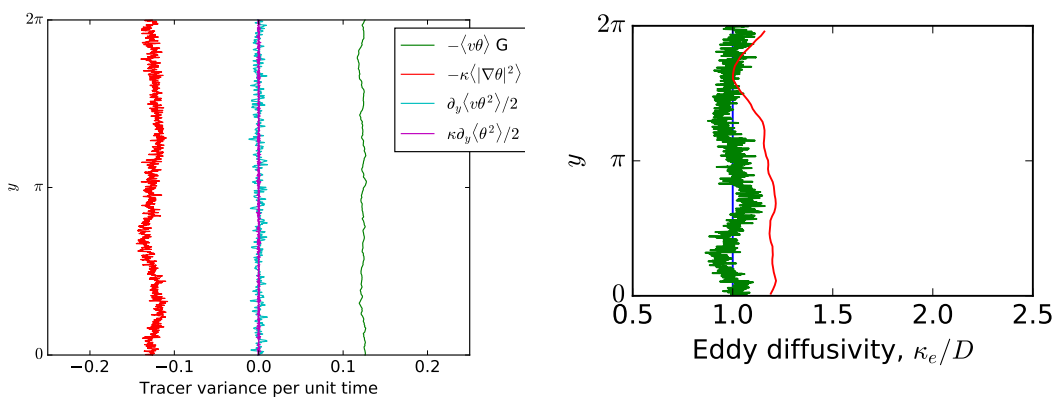


Figure 8: Results for $p = 2$ experiment: Tracer variance budget (left) and estimates of eddy diffusivity (right).

2.7 Advection-diffusion with a simple large-scale source

We employ a simple large-scale source

$$S(y) = \cos\left(\frac{2\pi}{L_y}y\right). \quad (33)$$

Because the source is only a function of y , half of the source is performed after the x -advection substep

$$\theta^{n+1/2} = \theta^{n+1/2} + \frac{\Delta t}{2}S(y). \quad (34)$$

The other half of the source could be applied in the same fashion, after the y -advection substep

$$\theta^{n+1} = \theta^{n+1} + \frac{\Delta t}{2}S(y). \quad (35)$$

In principle (35) is a brutal way to apply the source since source term is not invariant in y . To apply the source more accurately, we note that in the “ y -advection”+“half-source” substeps, we are solving

$$\theta_t + v(x)\theta_y = \cos\left(\frac{2\pi}{L_y}y\right), \quad (36)$$

which can be easily integrated along the characteristics $y = y_0 + v\Delta t/2$, to give

$$\theta(x, y, t + \Delta t) = \theta(x, y, \Delta t) + \frac{\sin[k_1(y_0 + v\Delta t/2)] - \sin k_1 y_0}{k_1 v}. \quad (37)$$

where $k_1 \stackrel{\text{def}}{=} \frac{2\pi}{L_y}$. We anticipate loss of accuracy for in regions where $v \approx 0$. To avoid this inaccuracies, we identify these points numerically, and use the exact value in limit $\Delta t \rightarrow 0$. This limit can be calculated using the L'Hospital rule, simply expanding about $v = 0$, to obtain

$$\frac{\sin[k_1(y_0 + v\Delta t/2)] - \sin k_1 y_0}{k_1 v} \rightarrow \frac{\Delta t}{2} \cos k_1 y_0 \quad \text{as} \quad v \rightarrow 0. \quad (38)$$

2.8 Mean tracer concentration

The x -averaged equation tracer equation is

$$\langle \theta \rangle_x = \cos k_1 y + (\kappa_e + \kappa) \partial_y^2 \langle \theta \rangle_x, \quad (39)$$

where we used an eddy diffusivity to parameterize the tracer flux with the eddy diffusivity $\kappa_e \gg \kappa$. In statistical steady state, averaging either in time or over ensembles, we obtain, to $\mathcal{O}(\kappa/\kappa_e)$,

$$\kappa_e \partial_y^2 \langle \theta \rangle_{x,t} = -\cos k_1 y, \quad (40)$$

Thus,

$$\langle \bar{\theta} \rangle = \frac{\cos k_1 y}{\kappa_e k_1^2}. \quad (41)$$

To obtain a prediction for the mean concentration, we use the the exact eddy diffusivity, given by the Einstein's formula:

$$\kappa_{ein} = \frac{\langle (\Delta x)^2 \rangle}{2\tau} = \frac{u_{rms}^2 \tau}{4}. \quad (42)$$

Figure 9 shows a comparison between the prediction given by (41) and numerical results from RW simulations. With enough scale separation between the large scale source and the eddies, there is spectacular agreement between theory and numerics, independent of the slope of the kinetic energy spectrum (see figure 9 top). Even without scale separation (i.e., when eddy

diffusivity is not formally justified), the time average of the x -averaged tracer concentration is reasonably consistent with the theoretical prediction. However, there are visible discrepancies between snapshots of x -averaged tracer concentration and the theoretical prediction; the discrepancies between snapshot and theory are larger with steep kinetic energy spectral slope since there is less self-averaging performed by the x -averaged operation.

3 Diffusion suppression by a mean flow

To study the suppression of eddy diffusivity by a mean flow, we simply add a constant zonal velocity to (14) and (15). The x -advection on the lattice is only slightly changed:

$$\begin{aligned}\dot{x} &= U + u(y), [0, \tau/2] : x = x_0 + [U + u(y)] \frac{\tau}{2}. \\ \dot{y} &= 0, [0, \tau/2] : y = y_0.\end{aligned}\quad (43)$$

The y -advection is

$$\begin{aligned}\dot{x} &= U, [\tau/2, \tau] : x = x_0 + U\tau/2. \\ \dot{y} &= v(x), [\tau/2, \tau] : \dot{y} = v(x_0 + U\tau/2).\end{aligned}\quad (44)$$

Hence

$$y = y_0 + C \sum_{j=j_{min}}^{j_{max}} \left(\frac{j}{j_{min}} \right)^{-p/2} \frac{1}{Uk} [\sin(k(x + U\tau)j + \psi_j) - \sin(k(x + U\tau/2)j + \psi_j)], \quad (45)$$

The mean square displacement is

$$\langle (\Delta y)^2 \rangle = C^2 \sum_j \left(\frac{j}{j_{min}} \right)^{-p} \left[\frac{1 - \cos(Uk\tau/2)}{(Uk)^2} \right]. \quad (46)$$

Note that in the limit of small mean velocity, $Uk\tau/2 \rightarrow 0$, we obtain the mean-square displacement for the non-mean-flow case:

$$\langle (\Delta y)^2 \rangle = u_{rms}^2 \frac{\tau^2}{2}. \quad (47)$$

We can then define the nondimensional parameter

$$\beta(U, p, j_{min}, j_{max}) = \frac{C^2 \sum_j \left(\frac{j}{j_{min}} \right)^{-p} \left(\frac{1 - \cos(Uk\tau/2)}{(Uk)^2} \right)}{u_{rms}^2 \frac{\tau^2}{2}} = \frac{2 \sum_j \left(\frac{j}{j_{min}} \right)^{-p} \left(\frac{1 - \cos(Uk\tau/2)}{(Uk\tau/2)^2} \right)}{\sum_j \left(\frac{j}{j_{min}} \right)^{-p}}, \quad (48)$$

which is a measure of suppression (no suppression with $\beta = 1$, full suppression with $\beta = 0$). Figure 10 shows β as a function of the mean flow speed U and the kinetic energy spectrum exponent p for different maximum wavenumber j_{max} . Flows with shallow kinetic energy spectrum are significantly suppressed by the mean flow. This is because for these flows, the small scales dominate the stirring, but the small scale eddies are significantly swept by the mean flow. In this local stirring regime, the relevant bulk non-dimensional number is

$$Uk_{max}\tau/2, \quad (49)$$

which can be large even when U is very small. On the other hand, flows with steep kinetic energy spectrum, the stirring is non-local and the relevant bulk non-dimensional parameter is

$$Uk_{min}\tau/2, \quad (50)$$

and the eddy turn-over time scale of the energy containing eddies relatively large compared to the mean advective time-scale, so that a significantly large mean flow is necessary to suppress the eddy diffusivity.

Figure 11 shows the β as a function of wavenumber and mean flow speed, that is

$$\beta(U, k) = \frac{2 \sum_j \left(\frac{j}{j_{min}} \right)^{-p} \left(\frac{1 - \cos(Uk\tau/2)}{(Uk\tau/2)^2} \right)}{\sum_j \left(\frac{j}{j_{min}} \right)^{-p}}, \quad (51)$$

where $k = 2\pi j/L_x$, and p is prescribed. Consistent with the discussion above, the eddy diffusivity at high wavenumbers are significantly more suppressed in flows with shallow kinetic energy spectrum.

4 RW revisited: spectral solutions

Here we solve the advection-diffusion equation in a double periodic domain marching forward with fourth-order time stepper. The main difference between this approach and the lattice model in Section 2 is that the diffusion is applied continuously instead of pulses. Indeed, an exponential time difference scheme, the diffusion is exact. As discussed in appendix A, the pulsing of the diffusion is the main source of error in the lattice model. This significantly reduces the numerical error rendering the overall solution and diagnostics more accurate (see figure ??). The main downside of this approach are the problems associated with numerical stability of the time marching scheme. In particular, for the experiment discussed here, numerical stability requires about 200 timesteps renovation cycles.

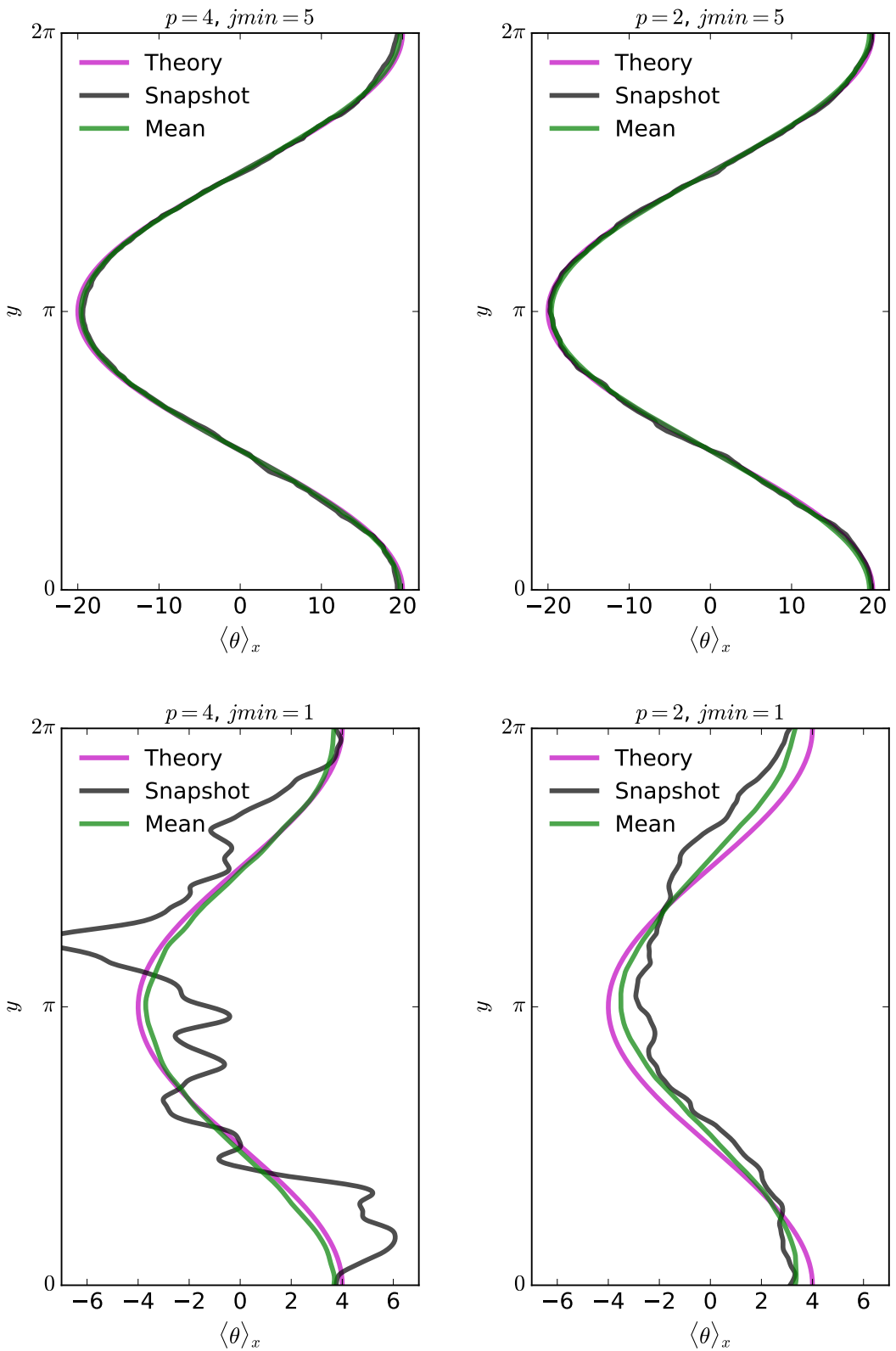


Figure 9: x -averaged tracer concentration simulated in 512×512 RW simulation with $\kappa = 5 \times 10^{-4}$, with $j_{min} = 5$ (top) and $j_{min} = 1$ (bottom).

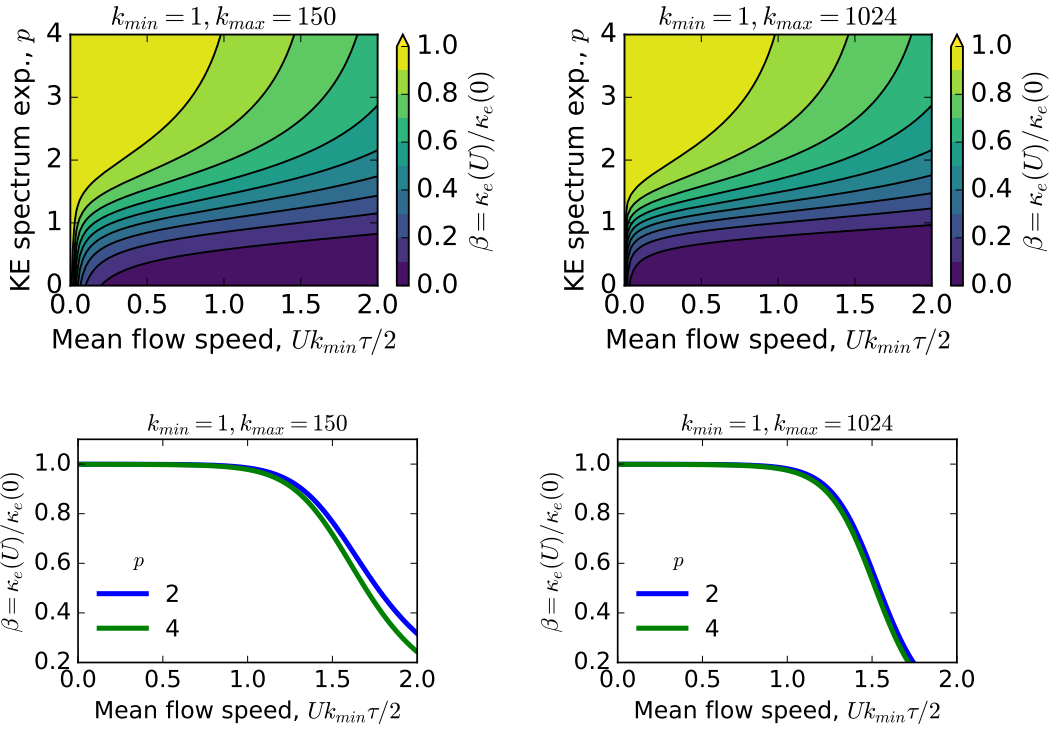


Figure 10: The parameter ratio of eddy diffusivity with mean flow relative to no-mean-flow eddy diffusivity. (Upper panels) Contours of β as a function of the mean flow (U) and kinetic energy exponent (p), with $k_{max} = 150$ (left) and $k_{max} = 1024$ (right). (Lower panels) A cut through the relevant exponents $p = 2$ and $p = 4$.

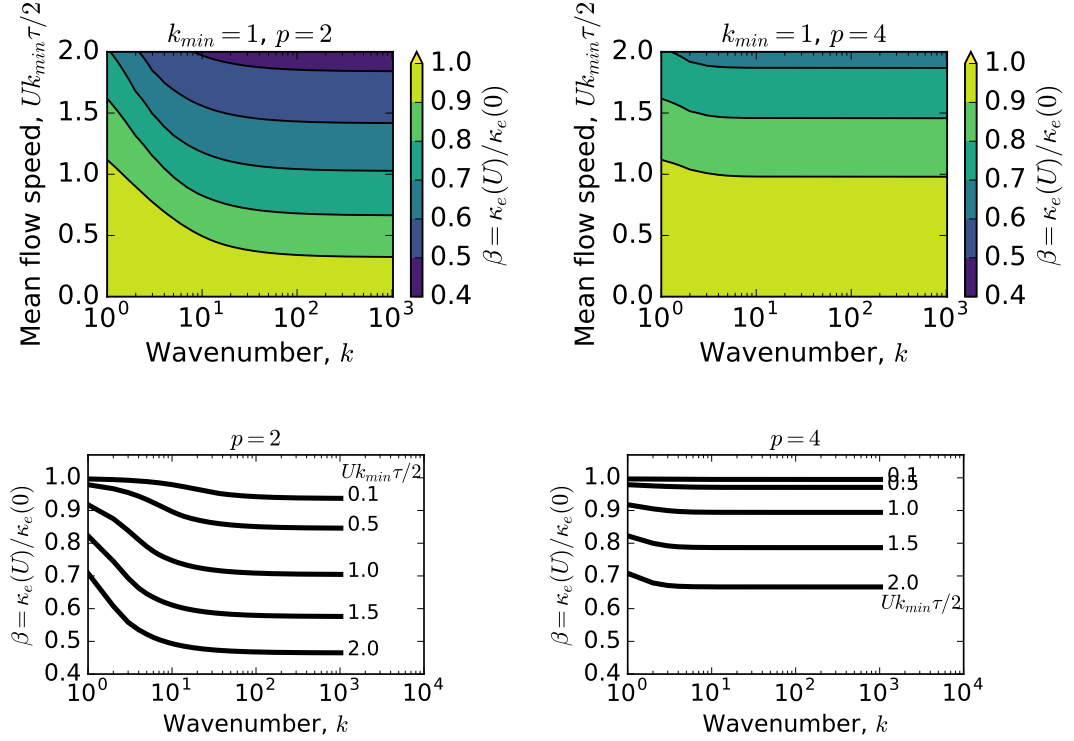


Figure 11: The parameter ratio of eddy diffusivity with mean flow relative to no-mean-flow eddy diffusivity. (Upper panels) Contours of β as a function of the mean flow (U) and wavenumber for two kinetic energy spectral exponents: $p = 2$ (left) and $p = 4$ (right). (Lower panels) A cut through different mean flow speeds.

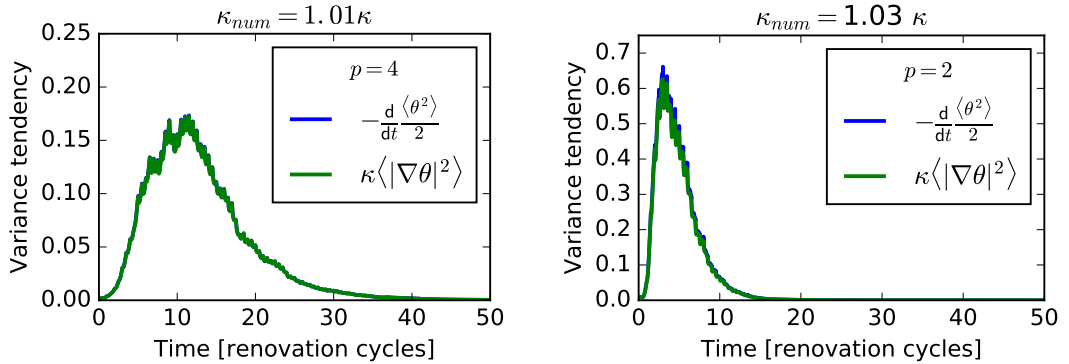


Figure 12: Time series of variance tendency and dissipation in a RW initial value problem advected spectrally and marched forward using a ETD-RK4 scheme. There is visually no difference between the two curves (Numerical diffusion in these solutions are rather insignificant).

A Caveats of the RW model

A.1 Biases

This is an approximate nature of the RW model, particularly the pulsing of the diffusion, has consequences for estimating diagnostics. For instance, if one estimates the tracer dissipation after the diffusion is applied, then these estimates will be biased low. Conversely, estimating the tracer dissipation before the diffusion is applied leads to a systematic overestimation of the tracer dissipation. Breaking up the steps in smaller substeps alternating advection with diffusion, and calculating the diagnostics before and after the diffusion is applied significantly reduces these biases. Unless otherwise stated, we used the following algorithm for the simulations described here:

Twice

$\frac{1}{2}$ x-advection

$\frac{1}{4}$ diffusion

Diagnostics

Twice

$\frac{1}{2}$ y-advection

$\frac{1}{4}$ diffusion

Diagnostics

We found that in some simulations there is biases related to the pulsing of diffusion significant biases may persist, particularly at relatively large κ and shallow velocity spectrum. To understand that consider the advection velocity field $(u, v) = (0, \alpha x)$. This can thought of the y-advection/diffusion sub-step with

$$\theta_t + \alpha x \theta_y = \kappa \Delta \theta, \quad (52)$$

where α is the rate of strain of the flow. Solutions to (52) have the form

$$\theta(x, y, t) = A_c(t) e^{i[(k - \alpha l)t]x + ly}, \quad (53)$$

where

$$A_c(t) = A(0) \exp\{-\kappa [(k^2 + l^2)t - kl\alpha t^2 + \alpha^2 l^2 t^3/3]\}. \quad (54)$$

Above we used the subscript c to denote that the diffusion is being applied continuously. After a substep $\tau/2$ we have

$$A_c(\tau/2) = A(0) \exp\{-\kappa [(k^2 + l^2)\tau/2 - kl\alpha\tau^2/4 + \alpha^2 l^2 \tau^3/24]\}. \quad (55)$$

If the diffusion is pulsed instead, we have

$$\begin{aligned} A_p(\tau/2) &= A(0) \exp\{-\kappa [(k - \alpha l\tau/2)^2 + l^2] \tau/2\} \\ &= A(0) \exp\{-\kappa [(k^2 + l^2)\tau/2 - kl\alpha\tau^2/2 + \alpha^2 l^2 \tau^3/8]\}. \end{aligned} \quad (56)$$

Note that pulsing the diffusion can underestimate or overestimate the solution. In particular,

$$\frac{A_p}{A_c} = \exp[\kappa l \alpha \frac{\tau^2}{2} (k - \alpha l \tau/6)]. \quad (57)$$

A.2 Numerical diffusion

In some simulations there is a remaining bias that we account for in the form of a ‘‘numerical diffusivity’’. To estimate this numerical diffusion we consider the global variance budget in initial value problems (IVPs). Figure 13 shows that the decay of variance in IVPs is faster than predicted by the tracer dissipation with molecular diffusivity. Numerical diffusivities estimated by linear algebra regression are 1.1κ and 1.8κ for $p = 4$ and $p = 2$, respectively. Accounting for the numerical diffusivity significantly reduces biases in eddy diffusivity estimates (see figure xyz).

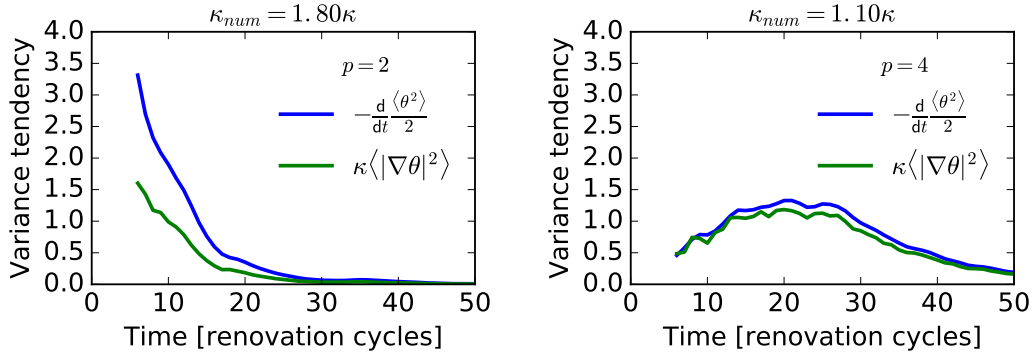


Figure 13: Time series of variance tendency and tracer dissipation for simulations of initial value problems with $p = 2$ and $p = 4$. Note that the decay of the variance decays faster than predicted by the tracer dissipation with molecular diffusivity.

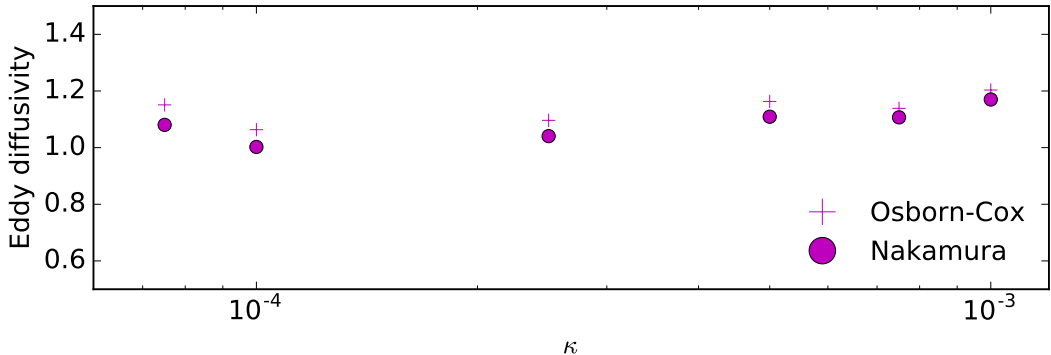


Figure 14: Sensitivity of eddy diffusivity estimates with steep kinetic energy spectrum $p = 4$ to small scale diffusivity.

B Derivation of Nakamura’s Eddy Diffusivity

The Nakamura effective diffusivity arises when transforming the diffusion equation into a area/-contour coordinate system, i.e. $A = A(\Theta, t)$, where A is the area bounded by the contour Θ at time t . Because the area bounded by a contour Θ is a well-defined graph, i.e. $\Theta = \Theta(A, t)$ (see

figure 15), we have¹

$$\Theta = \theta[A(\Theta, t), t], \quad (58)$$

so that

$$\frac{\partial \theta}{\partial A} A_t + \theta_t = 0 \quad \text{and} \quad \frac{\partial \theta}{\partial A} \frac{\partial A}{\partial \Theta} = 1. \quad (59)$$

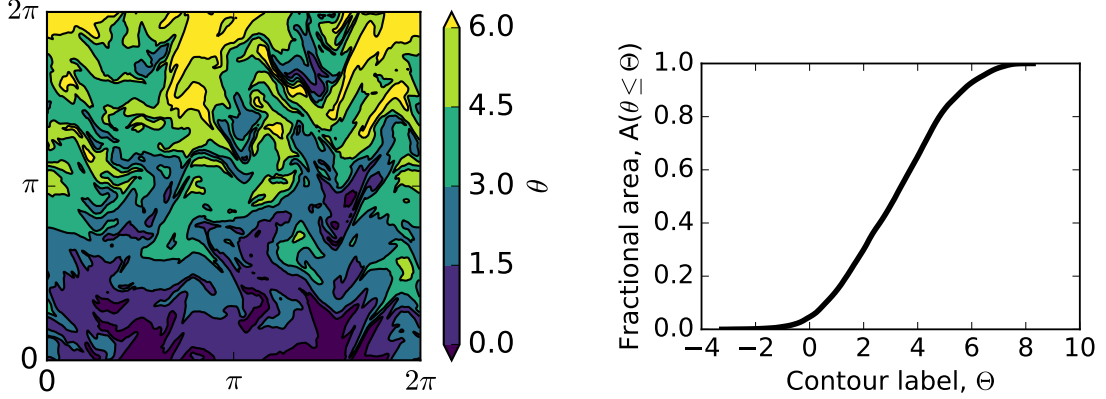


Figure 15: (Left) A snapshot of tracer concentration θ from a simulation of the RW model. (Right) The fractional area of tracer concentration satisfying $\theta \leq \Theta$, that is, the cumulative distribution function of θ .

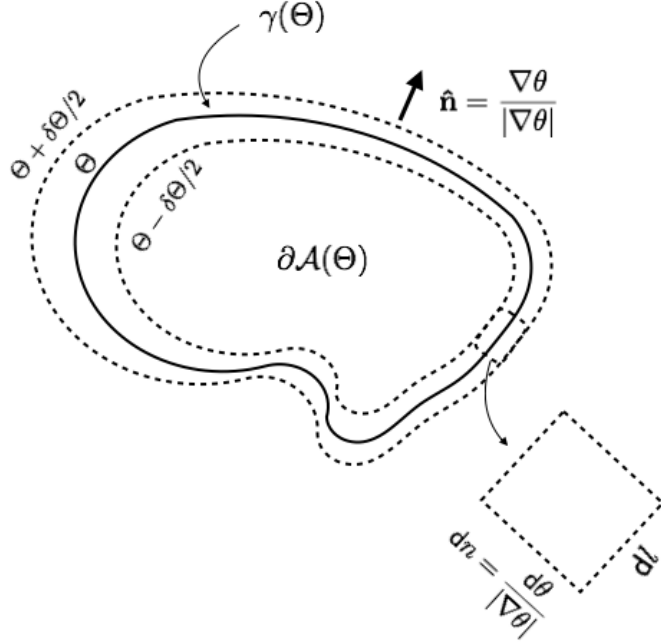


Figure 16: Schematics of the coordinate system defined by the the tracer contour $\theta = \Theta$.

¹It is very important to keep track of the difference between the tracer field θ and tracer contours defined by the label $\theta = \Theta$. It is irritating that a third of the oceanographic literature in this topic systematically confused θ with Θ in their derivations. Another third randomly makes the same confusion. The last third only occasionally changes a θ with Θ .

The integral of the scalar function f over the surface within the curves $\gamma(\Theta + d\Theta/2)$ and $\gamma(\Theta - d\Theta/2)$ (see figure B) is²

$$\delta I_\Theta(f) = \iint_{\partial A^+} f \, dx dy - \iint_{\partial A^-} f \, dx dy = \delta\theta \oint_\gamma f \frac{dl}{|\nabla\theta|}. \quad (60)$$

where $\partial A^+ = \partial A(\Theta + \delta\Theta/2)$ and $\partial A^- = \partial A(\Theta - \delta\Theta/2)$. Thus in the limit $\delta\Theta \rightarrow 0$,

$$\frac{\partial}{\partial\Theta} I_\Theta(f) = \frac{\partial}{\partial\Theta} \iint_{\partial A} f \, dx dy = \oint_\gamma f \frac{dl}{|\nabla\theta|}. \quad (61)$$

In particular, the specific case $f = 1$ gives:

$$\frac{\partial}{\partial\Theta} A = \oint_\gamma \frac{dl}{|\nabla\theta|}, \quad (62)$$

where the total area of the surface bounded by Θ is $A = I_\Theta(1)$. The thickness average of f along the $\gamma(\Theta)$ is defined by

$$\langle f \rangle_\Theta \stackrel{\text{def}}{=} \frac{\oint_\gamma f \frac{dl}{|\nabla\theta|}}{\oint_\gamma \frac{dl}{|\nabla\theta|}} = \frac{\partial}{\partial A} I_\Theta(f). \quad (63)$$

With the results above, we are ready to transform the advection-diffusion equation onto a coordinate system defined by the countour Θ . First, we note that the rate of change of the material surface A is given by

$$A_t = \oint_\gamma \mathbf{u}_c \cdot \hat{\mathbf{n}} \, dl, \quad (64)$$

where the velocity of the contour, locally normal to the contour, is defined by³

$$\mathbf{u}_c = -\theta_t \frac{\nabla\theta}{|\nabla\theta|^2} = -\frac{\theta_t}{|\nabla\theta|} \hat{\mathbf{n}}. \quad (65)$$

Thus, using the advection-diffusion equation (1), we obtain

$$\begin{aligned} \frac{\partial A}{\partial t} &= -\oint_\gamma \theta_t \frac{dl}{|\nabla\theta|} = \oint_\gamma \nabla \cdot (\mathbf{u}\theta) \frac{dl}{|\nabla\theta|} - \kappa \oint_\gamma \Delta\theta \frac{dl}{|\nabla\theta|} - \oint_\gamma S \frac{dl}{|\nabla\theta|} \\ &= \underbrace{\frac{\partial}{\partial\Theta} \iint_{\partial A} \nabla \cdot (\mathbf{u}\theta) \, dA}_{=0} - \kappa \underbrace{\frac{\partial}{\partial\Theta} \iint_{\partial A} \Delta\theta \, dA}_{=\oint_\gamma |\nabla\theta|^2 \frac{dl}{|\nabla\theta|}} - \frac{\partial}{\partial\Theta} \iint_{\partial A} S \, dA. \end{aligned} \quad (66)$$

Now using (59) we obtain

$$\begin{aligned} \frac{\partial\theta}{\partial t} &= \kappa \frac{\partial}{\partial A} \iint_{\partial A} \Delta\theta \, dA + \frac{\partial}{\partial A} \iint_{\partial A} S \, dA \\ &= \frac{\partial}{\partial A} \left(K_n(A, t) \frac{\partial\theta}{\partial A} \right) + \langle S \rangle_\Theta, \end{aligned} \quad (67)$$

where the effective diffusivity is

$$K_n(A, t) = \frac{\kappa \oint_\gamma |\nabla\theta| \, dl}{\partial\theta/\partial A} = \kappa \underbrace{\frac{\partial A}{\partial\Theta}}_{\oint_\gamma \frac{dl}{|\nabla\theta|}} \oint_\gamma |\nabla\theta| \, dl = \frac{\partial A}{\partial\Theta} \frac{\partial}{\partial A} \iint_{\partial A} \kappa |\nabla\theta|^2 \, dx dy = \frac{\langle \kappa |\nabla\theta|^2 \rangle_\Theta}{(\partial\theta/\partial A)^2}. \quad (68)$$

²We can also use the fundamental theorem of calculus to obtain $I_\Theta(f) = \int_{\theta \leq \Theta} \oint_\gamma f \frac{dl}{|\nabla\theta|}$.

³Note that for the contour $\Theta = \theta[\mathbf{x}(t), t]$ we have $\theta_t + \mathbf{u}_c \cdot \nabla\theta = 0$, where $\mathbf{u}_c \stackrel{\text{def}}{=} d\mathbf{x}/dt$.

Note that the effective diffusivity has units of $(\text{length})^4 \times (\text{time})^{-1}$. The Nakamura eddy diffusivity is defined by

$$\kappa_n(\Theta, t) = \frac{K_e}{L_{min}^2} = \frac{L_{eq}^2}{L_{min}^2} \kappa, \quad (69)$$

where the “equivalent length” is

$$L_{eq}^2 \stackrel{\text{def}}{=} \underbrace{\oint_{\gamma} \frac{dl}{|\nabla \theta|}}_{\stackrel{\text{def}}{=} I_2} \underbrace{\oint_{\gamma} |\nabla \theta| dl}_{\stackrel{\text{def}}{=} I_1}, \quad (70)$$

where the alternative expressions (useful for numerical computations) for the integrals are

$$I_2 = \frac{\partial}{\partial \Theta} \iint_{\partial A} dx dy, \quad \text{and} \quad I_1 = \frac{\partial}{\partial \Theta} \iint_{\partial A} |\nabla \theta|^2 dx dy, \quad (71)$$

Note that κI_1 is proportional to the dissipation rate within contours. The tracer dissipation rate, averaged along the contours, is what mainly determines the eddy diffusivity. The integral I_2 is merely a constant determined by the geometry of the problem.

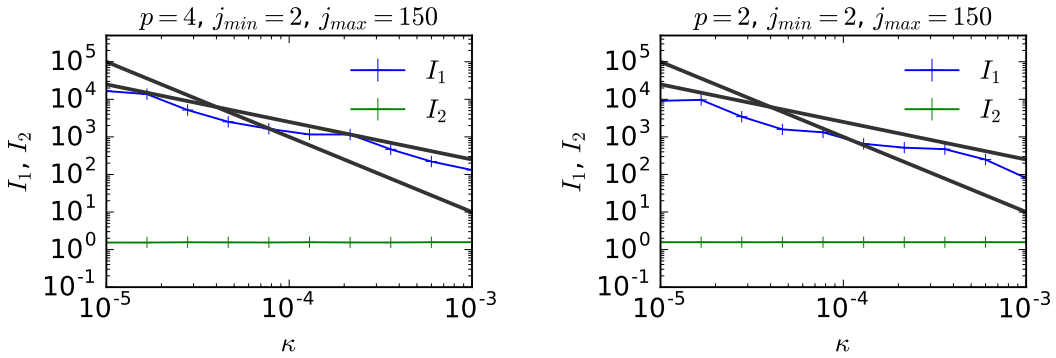


Figure 17: Numerical estimates of the integral I_1 and I_2 as a function of the small scale diffusivity. These integrals are based only

Also in (69), L_{min} is the minimum (unstrained) length of the contour. In simple domains such as a periodic channel, L_{min} is unambiguously defined as the length of the channel. In more complicated realistic geometry and source functions, the definition of L_{min} may not be straightforward. In practice, one can estimate L_{min} by calculating L_{eq} in simulations with large Peclet number ($\kappa_n \rightarrow \kappa$). In the oceanographic literature L_{eq} is commonly mistaken by the length of the contour (e.g., Ferrari and Nikurashin, 2010). This is only true if $|\nabla \theta|$ is constant, and represents a lower bound on L_{eq} , obtained using the Cauchy-Schwartz inequality⁴:

$$L_{eq}^2 \geq L^2 = \left(\oint_{\gamma} dl \right)^2. \quad (72)$$

While the equivalent length notation above provides a useful interpretation, in practice one does not compute line integrals. Instead, the third equality in (68) suggests a straightforward numerical approximation

$$K_e(\Theta, t) \approx \frac{\delta I_{\Theta}(1)}{(\delta \Theta)^2} \delta I_{\Theta}(\kappa |\nabla \theta|^2), \quad (73)$$

⁴ $\oint_{\gamma} f^2 dl \oint_{\gamma} g^2 dl \geq \left(\oint_{\gamma} f g dl \right)^2$.

where $\delta I_\theta(f)$ is the approximate area integral of f within the contours $\Theta + d\Theta/2$ and $\Theta - d\Theta/2$ (see figure 5). These approximate integrals are computed simply by counting pixels:

$$\delta I_\theta(f) = \sum_j f dx dy, \quad \Theta - d\Theta/2 \leq \theta \leq \Theta + d\Theta/2, \quad (74)$$

where the summation on j represents the pixels within the contour. In practice the diagnostic is not very sensitive to the contour spacing $d\Theta$.

Finally note that the Nakamura diffusivity is a function of the the contour Θ (or equivalently of the area bounded by the contour). With simple geometry of initial conditions and source function, $\kappa_N(\Theta, t)$ can be mapped to physical space, e.g. as direction of the tracer gradient or the equivalent latitude.

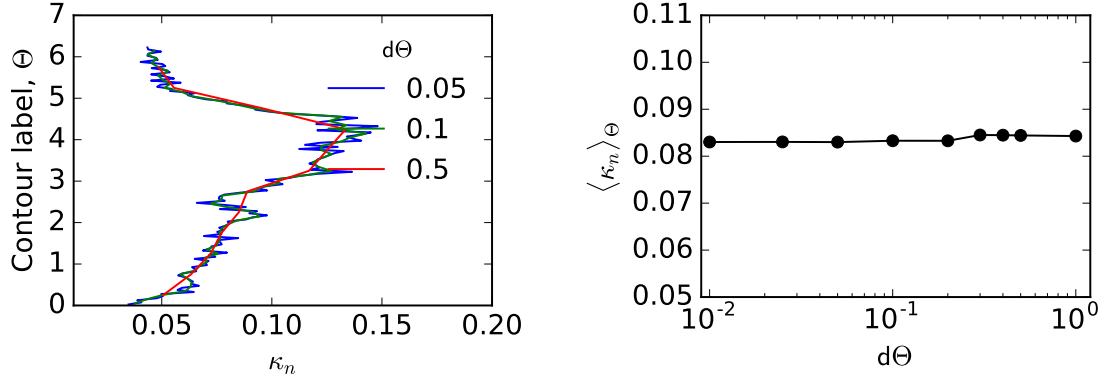


Figure 18: Sensitivity of the Nakamura diffusivity estimate to the contour spacing $d\Theta$. In this example, the Nakamura eddy diffusivity was computed for a single snapshot in Figure 15a.